A Switched Reluctance Motor Torque Ripple Reduction Strategy with Deadbeat Current Control and Active Thermal Management

Xing Zhang, *Senior Member, IEEE*, Qingqing Yang, *Student Member, IEEE*, Mingyao Ma, *Member, IEEE*, Zhengyu Lin, *Senior Member, IEEE* and Shuying Yang, *Member, IEEE*

***Abstract*—This paper presents a switched reluctance motor (SRM) torque ripple reduction strategy with deadbeat current control and active thermal management. In this method, the SRM torque is indirectly controlled by the phase current. A deadbeat current control method is used to improve the SRM phase current control accuracy, so that SRM torque control error can be reduced significantly. According to the online measurement of the power switching device temperature, the switching frequency will be reduced to prevent the SRM power converter from being damaged by over-temperature. The feasibility and effectiveness of the proposed strategy have been verified in both simulation and experimental studies.**

***Index Terms*—Switched reluctance motor (SRM), deadbeat control, torque ripple reduction, active thermal management.**

I. Introduction

Over the last two decades, electric vehicles (EVs) and hybrid electric vehicles (HEVs) have attracted increasing attention[1]-[3]. Permanent magnet (PM) motor is one of the most popular electric motors in applications of EVs/HEVs, but has potential issues for mass production due to the scarcity of rare-earth materials[4]. In addition, permanent magnet materials will suffer from magnetic deterioration under high temperature, vibration and overcurrent conditions, which will damage the motor seriously and affect the safe operation of EVs/HEVs.

Switched reluctance motors (SRM) have attracted more and more attention for research and industrial applications, due to the advantages of rare-earth-free feature, high efficiency, robust structure, excellent fault tolerance operation, high starting torque for initial acceleration, and so on[5]–[8]. Consequently, SRMs have been considered as a promising candidate for EVs /HEVs applications. At present, SRMs have been used in some EVs/HEVs on the market, such as Holden's ECOmmodore and Xiamen Jinlong's XMQ6125G hybrid city bus, etc. However, because of double-saliency structure of SRMs, high torque ripples and noise are the inherent issues caused by normal force fluctuations during phase current excitations[9]-[10], which limits SRMs in the EVs/HEVs applications with high performance requirements. Thus, SRM torque ripple reduction techniques are necessary for EVs/HEVs applications. At high speed range, the angle interval position of the conduction interval is the core factor for determining the SRM output performance. Therefor angle position control method is usually used to reduce torque ripple. To reduce torque ripple at low speed range, various schemes have been proposed in recent years[11]–[19], and direct instantaneous torque control (DITC) and torque-sharing function (TSF) are two common solutions. DITC has advantage of simple structure, but it requires complex switching rules for smoothing torque ripples during the commutation period[12].

TSF based torque ripple reduction methods have advantages of simple control structure and easy implementation[13]. Several TSF methods have been reported, such as linear, cubic, and exponential TSFs, and can be implemented offline or online. In [12], a nonlinear logical TSF for torque ripple reduction and efficiency enhancement is introduced. In [14] and [15], an iterative learning controller is proposed to add a compensation current to the current reference to reduce the torque ripple resulting from the nonlinearity of an SRM. In [16], turn-on angle of an adaptive TSF is adjusted with the speed in order to reduce torque ripple. In [19], the shape of proposed TSF is flexible, and not limited to a specific type. The objective function of the proposed TSFs directly combines the squares of the phase current and derivatives of current reference with a Tikhonov factor.

Most of the TSFs mentioned above implement torque control by phase current control, which require accurate phase current controllers. Hysteresis current controller (HCC) is a simple way to track the nonlinear current reference. When implemented with micro-controller, it has a good control performance with high switching frequency. However, in the high-power applications, the switching frequency is limited by the comprehensive factors such as the switching power loss and reliability of the switch device. It is difficult to implement high performance current control under HCC with the limited switching frequency.

Deadbeat control (DBC) methods have been used to track the torque and flux linkage of SRM[20]. In this paper, a novel deadbeat current control method integrated into the SRM phase current controller, which can improve the current control accuracy with a low switching frequency for high-power SRM drive systems. The deadbeat control method can predict the duty cycle of the switching signal for the next control period according to current error, and achieve an accurate current tracking. Thus, the method can reduce the SRM torque ripple for TSF based torque ripple reduction

methods.

For the safety operation of EVs/HEVs systems, a reliable power converter for SRM drive systems is important. The thermal reliability of power converters is becoming more and more important with increasing the power capacity and switching frequency of power electronic device. At present, many insulated gate bipolar transistor (IGBT) modules have temperature feedback function. To take advantage of this function, some effective technologies have been proposed to avoid over-temperature failure of power converter, mainly following two methods: derating and switching frequency reduction. However, the derating methods will lead to insufficient power and even affect the safety of EVs/HEVs[21]. The switching frequency reduction method will reduce the current control performance, and cause the high torque ripple of SRM and affect the comfort of EVs/HEVs[22] with traditional control method.

This paper proposed to use deadbeat current control method to improve the SRM phase current control accuracy under low switching frequency, therefore, switching frequency reduction can be used in the proposed active thermal management for power switching devices. The switching frequency can be adjusted according to the feedback temperature of IGBT module to prevent IGBTs from over-temperature failure, so the safety of EVs/HEVs can be improved. In order to validate the feasibility and effectiveness of the proposed control method, the simulation and experimental validations have carried out on a three-phase 12/8-pole 35 kW SRM.

II. Torque Sharing Function Control Of Switched Reluctance Motor With Active Thermal Management

Fig. 1 shows the block diagram of the proposed torque sharing function control of an SRM with active thermal management, which is mainly composed of an SRM, a power converter, an analog-to-digital converter (ADC), and a digital control system. The digital control system consists of a thermal controller and a TSF control module. The proposed active thermal management can be realized by the thermal controller, which can regulate switching frequency f according to converter temperature. In the drive system, the frequency of the digital control system and the ADC frequency are same as the switching frequency, so they change with the switching frequency. Each module of the block diagram will be described in detail below.

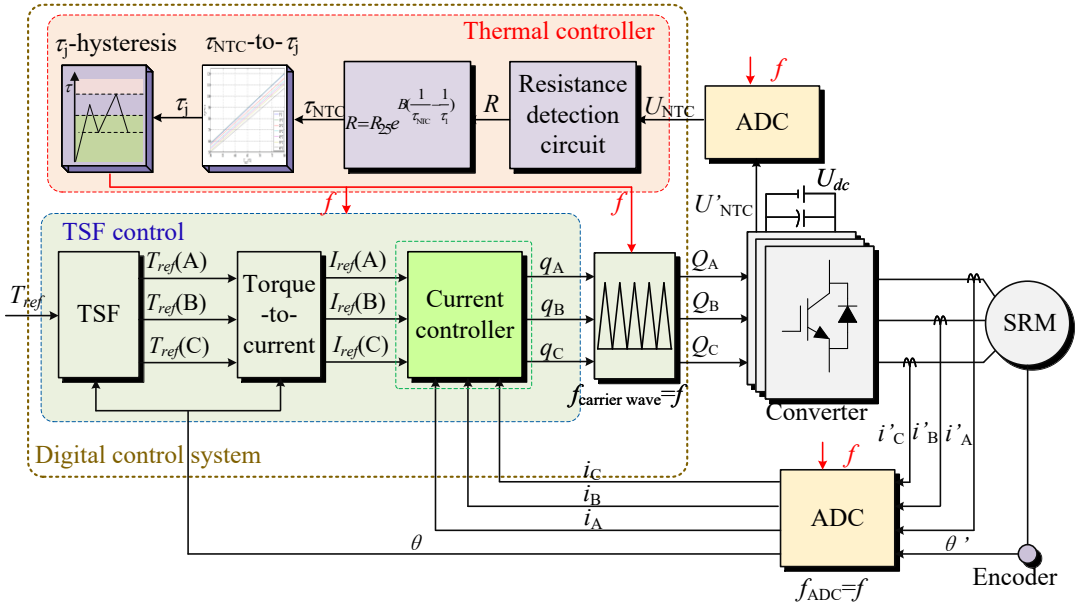

Fig.1 Block diagram of torque sharing function control of switched reluctance motor with active thermal management

A. The thermal controller

Asymmetric half-bridge converters are commonly used for SRM drive systems, as shown in Fig. 2. In practical, commercial IGBT modules are often used for high-power SRM drive systems. In many of the high power IGBT modules such as Infineon's EconnoDUAL™3 series, a negative thermal coefficient thermistor (commonly called NTC) is integrated in the package, as shown in Fig. 3, making it easy to measure the baseplate temperature in module. In this research, Infineon's IGBT module FF600R12ME4 is used to build the power converter for the SRM drive. Fig. 3 shows the structure of an IGBT module. For heat dissipation, a direct copper bonded (DCB) ceramic substrate is usually soldered to the baseplate, and the IGBT as well as diode silicon chips are then soldered to it. A NTC is also soldered to DCB. The instantaneous NTC-thermistor resistance value can be obtained by the resistance detection circuit, as shown in Fig. 1. Than the value can be used to obtain the instantaneous IGBT module temperature depending on the following equation[23].

$$R = R_{25} e^{B\left(\frac{1}{\tau_{NTC}} - \frac{1}{\tau_1}\right)} \tag{1}$$

where τ_{NTC} is NTC temperature, R is the instantaneous resistance value of NTC-thermistor, R_{25} is the rated resistance value of NTC-thermistor at 298.15K (SI), B is a constant that can be obtained from the datasheet, τ_1=298.15K[24]. When the power converter works, the instantaneous NTC temperature

τ_{NTC} can be calculated by taking the instantaneous resistance value R of NTC-thermistor into the upper equation (1).

IGBT junction temperature τ_j is an important parameter of the thermal controller. τ_j can be obtained from the τ_{NTC} to τ_j table, as shown in Fig. 1. Firstly, an off-line relationship table between water-cooled flow rate, ambient temperature, NTC temperature τ_{NTC} and IGBT junction temperature τ_j is established by experiment. Then, when electric vehicle runs, the junction temperature τ_j can be obtained accurately by looking up the off-line table, τ_{NTC}-to-τ_j talbe, according to the τ_{NTC}, water-cooled flow rate, ambient temperature.

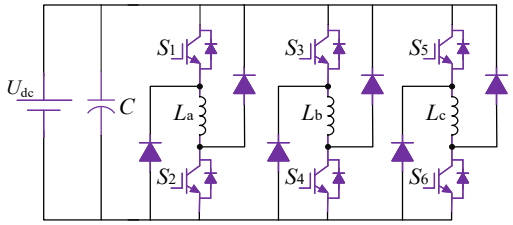

Fig.2 Topology of an asymmetric half-bridge converter

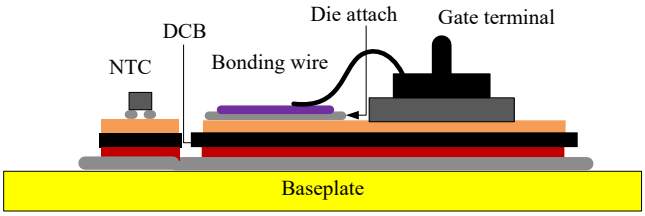

Fig.3 Cross-sectional view of IGBT modules

The working principle of the proposed active thermal management is to reduce the power switching frequency when the power switching device temperature is high. It will adjust IGBT switching frequency according to the junction temperature τ_j, as shown in Fig. 4. In this way, the temperature of the power converter can be controlled within a safe range.

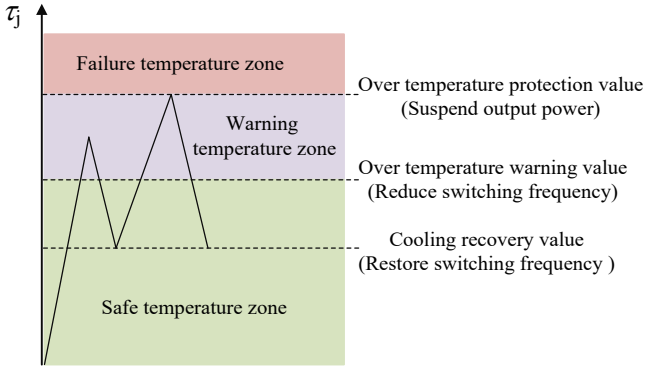

Fig.4 Power converter temperature active thermal management

In Fig. 4, the temperature range can be divided into safe temperature zone, warning temperature zone and failure temperature zone. In safe temperature zone, a higher switching frequency is adopted to achieve high performance output of SRM. Whenever the temperature of the power converter reaches the over temperature warning value, the switching frequency is reduced to prevent the power converter from over temperature. Normally, the temperature will decline after the switching frequency decreases. When the temperature drops to the cooling recovery value, the switching frequency is restored.

Vehicles are exposed to harsh environment and anything could happen throughout the life time so any other abnormal conditions should be considered as well to protect power converter from over temperature. For example, when the temperature reaches the over temperature warning value, fluctuating load condition may cause the temperature to continue to rise with low switching frequency. Additionally, cooling condition and any unexpected events may cause the temperature to exceed the over temperature protection value. In order to prevent from over temperature, the power converter is suspended at this time.

B. TSF control module

The SRM total output torque is composed of the sum of the torque generated by all phases at the same time. In order to produce a torque with low ripples, the total torque reference can be divided into individual phase torque references through TSF, as shown in equation (2). The torque reference of each phase can be obtained by equation (3).

$$f_M(\theta)=\begin{cases}0 & 0\le\theta\le\theta_{on}\\ f_{rise}(\theta) & \theta_{on}\le\theta\le\theta_{on}+\theta_{overlap}\\ 1 & \theta_{on}+\theta_{overlap}\le\theta\le\theta_{off}-\theta_{overlap}\\ f_{fall}(\theta) & \theta_{off}-\theta_{overlap}\le\theta\le\theta_{off}\\ 0 & \theta_{off}\le\theta\le\theta_{p}\end{cases} \quad (2)$$

$$T_{ref}(\mathrm{M})=T_{ref}\cdot f_M(\theta) \quad (3)$$

where T_{ref} is the total torque reference, T_{ref}(M) is the torque reference for Mth phase; $f_M(\theta)$ is the Mth phase TSF, $f_{rise}(\theta)$ is the rising TSF for the incoming phase, $f_{fall}(\theta)$ is the decreasing TSF for the outgoing phase; θ_{on}, θ_{off}, $\theta_{overlap}$ and θ_p are turn-on angle, turn-off angle, overlapping angle, and rotor pole pitch, respectively.

Linear and sinusoidal TSF methods are commonly used. The linear TSF has constant slope of torque in the commutation region. This method is simple, but it cannot reflect nonlinear torque production characteristics of SRM. Therefore, the torque ripple is increased around the beginning and end of commutation due to the higher nonlinear inductance slope. The sinusoidal TSF uses a sinusoidal curve during commutation, as shown in Fig. 5. This method is

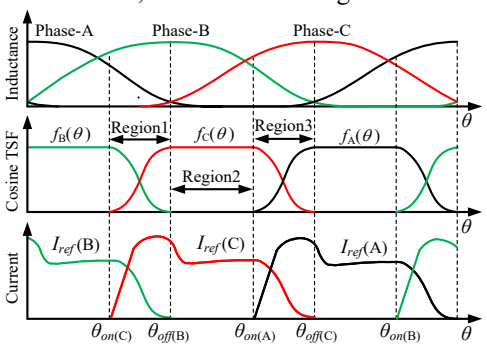

Fig.5 Phase inductances, sine TSF and phase current reference curves

similar to the non-linear inductance characteristics. Therefore, under this torque reference curve, the actual torque is easier to track the torque reference. Thus, the sinusoidal TSF is adopted in this paper.

In TSF control module, the input total torque reference T_{ref} is divided into individual torque references for each phase through TSF block with respect to rotor position. The separate torque references are converted to current references in the "Torque-to-current" block based on rotor position information. In traditional control method, a phase current controller HCC is used to track these current references.

III. A Deadbeat Control Method

For high-power applications, the power switching frequency is limited to reduce the switching power loss. In order to improve the SRM current control accuracy at low switching frequency conditions, a deadbeat current control method is proposed in this research.

A. Working principle of deadbeat control method

The deadbeat current control method is shown in Fig. 6.

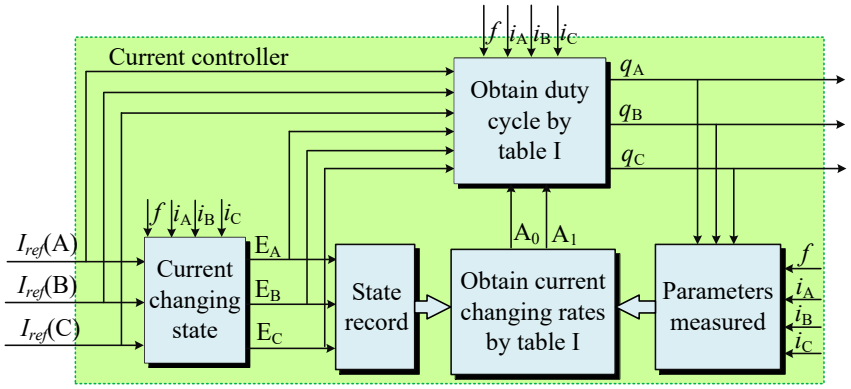

Fig.6 The deadbeat current control method

By neglecting mutual coupling phase, the phase voltage equation of an SRM can be given as

$$\begin{aligned} U &= r\cdot i+\frac{d\psi(\theta,i)}{dt}=r\cdot i+\frac{d[L(\theta,i)\cdot i]}{dt} \\ &= r\cdot i+i\cdot\frac{d[L(\theta,i)]}{dt}+L(\theta,i)\cdot\frac{di}{dt} \end{aligned} \tag{4}$$

where U is the voltage applied to the phase winding, r is the resistance of the winding, i is the current of phase, Ψ is the linkage flux, θ is the rotor position and L is the phase inductance.

In digital drive system, because switching period is very short, an assumption is made that phase inductance remains unchanged in a switching period. Thus, in the kth switching period, equation (4) can be expressed as

$$U(k)=r\cdot i(k)+L(k)\cdot\frac{i(k+1)-i(k)}{T_s} \tag{5}$$

where T_s is the switching period.

According to (5), when the freewheeling state is applied to the phase winding, the changing rate of the phase current A_0 in the kth switching period can be expressed as

$$A_0(k)=-\frac{r\cdot i(k)}{L(k)}=\frac{i(k+1)-i(k)}{T_s}\bigg|_{U=0} \tag{6}$$

Because in this state, the phase current change slowly, A_0 can be assumed to remain constant over a switching period.

When the phase voltage is bus voltage U_{dc} or negative bus voltage $-U_{dc}$, the voltage of r can be ignored. Thus, the changing rates of the phase current can be expressed as

$$A_1(k)=\frac{U_{dc}}{L(k)}=\frac{i(k+1)-i(k)}{T_s}\bigg|_{U=U_{dc}}\approx -A_2(k) \tag{7}$$

where A_1 and A_2 are the changing rates of the phase current, when the phase voltage is U_{dc} and $-U_{dc}$, respectively.

From equation (6) and equation (7), it can be concluded that the phase current varies linearly in a switching period regardless of whether the phase voltage is 0, $-U_{dc}$ or U_{dc}. Thus, changing rate of the phase current can be calculated according to the current change in a switching period.

The working principle of the deadbeat control method is shown in Fig. 7, where PWM_k^a indicates that the kth switching period of phase A electric cycle, similar with phase B and phase C. The following assumptions has been made for the design of the deadbeat control:

1) The SRM's three phases are identical.
2) The SRM speed is constant in a continuous three electric cycle, because the acceleration of SRM is limited by its inertia. Therefore, in a continuous three electric cycle, the current changing rates of these switching periods with the same serial number is equal, expressed as equation (8) and equation (9).

$$A_0(k)=A_{a0}(k)=A_{b0}(k)=A_{c0}(k) \tag{8}$$

$$A_1(k)=A_{a1}(k)=A_{b1}(k)=A_{c1}(k) \tag{9}$$

where $A_{a0}(k)$ and $A_{a1}(k)$ is the current changing rates in the kth switching period of phase A electric cycle; $A_{b0}(k)$ and $A_{b1}(k)$ is the current changing rates in the kth switching period of phase B electric cycle; $A_{c0}(k)$ and $A_{c1}(k)$ is the current changing rates in the kth switching period of phase C electric cycle; $A_0(k)$ and $A_1(k)$ is the current changing rates in the kth switching period of the continuous three electric cycle.

3) Turn-on angle and turn-off of each phase are the same in a continuous three electric cycle, respectively.

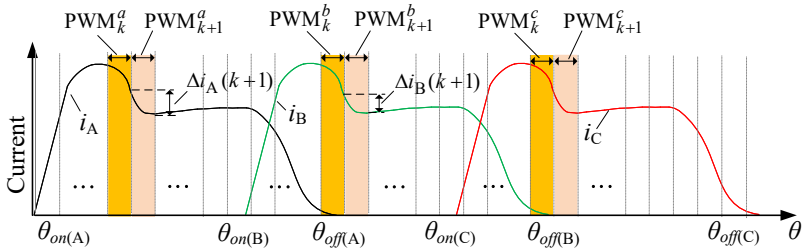

Fig.7 Control principle of deadbeat control method

Based on the above assumptions, online measured SRM running parameters of previous two phases can be used for the phase current control, and predict the required duty cycle of pulse width modulation (PWM) for the next switching period accurately.

When SRM starts, the duty cycles of the initial first two conducting phases cannot be predicted under DBC method because of the lack of previous two phases running parameters. In order to make the SRM start normally, the duty cycles of the initial first two conducting phases are set to the optimal value obtained by simulation. Then, the duty cycles can be predicted under DBC method from the next conducting phase. Thus, SRM can start smoothly.

In order to illustrate the DBC method, assume that SRM is being in the phase C conduction region. Thus, phase A and B have been excited, and the parameters of phase A and B have been known. These parameters include switching frequency f, duty cycle q, current variation $\triangle i$ and switching state E for each switching period. The switching state of "1" indicates that the magnetizing state or freewheeling state is in the switching period. The switching state of "-1" indicates that the demagnetizing state is in the switching period.

To predict the required duty cycle for the next switching period of phase C under DBC method, equation (10) and equation (11) are obtained using the above parameters. Then the equations (10) and (11) are combined and solved to obtain the changing rates of phase current $A_0(k+1)$ and $A_1(k+1)$.

$$\Delta i_A(k+1)=\begin{cases}\text{if } E_A(k+1)=1,\\ \dfrac{A_1(k+1)\cdot q_A(k+1)}{f}-\dfrac{A_0(k+1)\cdot(1-q_A(k+1))}{f}\\ \text{if } E_A(k+1)=-1,\\ -\dfrac{A_1(k+1)\cdot(1-q_A(k+1))}{f}-\dfrac{A_0(k+1)\cdot q_A(k+1)}{f},\end{cases} \tag{10}$$

$$\Delta i_B(k+1)=\begin{cases}\text{if } E_B(k+1)=1,\\ \dfrac{A_1(k+1)\cdot q_B(k+1)}{f}-\dfrac{A_0(k+1)\cdot(1-q_B(k+1))}{f}\\ \text{if } E_B(k+1)=-1,\\ -\dfrac{A_1(k+1)\cdot(1-q_B(k+1))}{f}-\dfrac{A_0(k+1)\cdot q_B(k+1)}{f}\end{cases} \tag{11}$$

where $q_A(k+1)$, $\triangle i_A(k+1)$ and $E_A(k+1)$ are duty cycle, current variation and switching state in the PWM$_{k+1}^a$ of phase A electric cycle, respectively. $q_B(k+1)$, $\triangle i_B(k+1)$ and $E_B(k+1)$ are duty cycle, current variation and switching state in the PWM$_{k+1}^b$ of phase B electric cycle, respectively.

For example, when $E_A(k+1)=1$ and $E_B(k+1)=-1$, the $\triangle i_A(k+1)$ in equation (10) is equal to the above polynomial, and $\triangle i_B(k+1)$ in equation (11) is equal to the below polynomial. Then a binary linear equation group is obtained by combining equations (10) and (11), expressed as equation (12). The changing rates of phase current $A_0(k+1)$ and $A_1(k+1)$ are obtained by solving equation (12).

$$\begin{cases}\Delta i_A(k+1)=\dfrac{A_1(k+1)\cdot q_A(k+1)}{f}-\dfrac{A_0(k+1)\cdot(1-q_A(k+1))}{f}\\ \Delta i_B(k+1)=-\dfrac{A_1(k+1)\cdot(1-q_B(k+1))}{f}-\dfrac{A_0(k+1)\cdot q_B(k+1)}{f}\end{cases} \tag{12}$$

Then, the phase C switching state $E_C(k+1)$ can be calculated using equation (13). The duty cycle $q_C(k+1)$ of the next switching period is obtained using equation (14).

$$E_C(k+1)=\begin{cases}1, & \text{if } I_{ref}(k+1)+\dfrac{A_0(k+1)}{f}\ge i_c\\ -1, & \text{if } I_{ref}(k+1)+\dfrac{A_0(k+1)}{f}<i_c\end{cases} \tag{13}$$

$$I_{ref}(k+1)-i_C=\begin{cases}\text{if } E_c(k+1)=1,\\ \dfrac{A_1(k+1)\cdot q_C(k+1)}{f}-\dfrac{A_0(k+1)\cdot(1-q_C(k+1))}{f}\\ \text{if } E_c(k+1)=-1,\\ -\dfrac{A_1(k+1)\cdot(1-q_C(k+1))}{f}-\dfrac{A_0(k+1)\cdot q_C(k+1)}{f}\end{cases} \tag{14}$$

Finally, the parameters in this switching period of phase C are recorded for the next phase duty cycle prediction. As an example, the DBC method is illustrated in phase C. The duty cycle prediction in other phase is in the same way as phase C.

B. Digital realization of the deadbeat control method

Taking the phase C current control as an example, the digital implementation of the proposed deadbeat control method is explained.

Firstly, the conducting phase is decided according to the position feedback of SRM.

Secondly, duty cycle, current variation and switching state in the $(k+1)$th switching period have been recorded for previous phase A and phase B current control. According to the values of $E_A(k+1)$ and $E_B(k+1)$, there are four

combinatorial states: (1,1), (1,-1), (-1,1) and (-1,-1). According to these combinatorial states, the changing rates of phase C current are achieved with equations in table I.

Then, the switching state $E_C(k+1)$ in the next switching period can be calculated with equation (13). According to the switching state $E_C(k+1)$, the duty cycle $q_C(k+1)$ of the next switching period is obtained with equations in table I.

Finally, the duty cycle $q_C(k+1)$ is converted to gate drive signal Q_C for the power convertor.

The flow chart of the deadbeat control method is shown in Fig. 8, and these equations used in the flow chart are shown in the table I.

TABLE I

EQUATIONS USED IN THE FLOW CHART

State	Equation
(1,1)	$\begin{cases} A_0(k+1)=\dfrac{\Delta i_A(k+1)\cdot q_B(k+1)-\Delta i_B(k+1)\cdot q_A(k+1)}{q_A(k+1)-q_B(k+1)}\cdot f \\ A_1(k+1)=\dfrac{\Delta i_B(k+1)\cdot f+A_0\left(1-q_B(k+1)\right)}{q_B(k+1)} \end{cases}$
(1,-1)	$\begin{cases} A_0(k+1)=\dfrac{\Delta i_A(k+1)\cdot(1-q_B(k+1))+\Delta i_B(k+1)\cdot q_A(k+1)}{-[(1-q_A(k+1))\cdot(1-q_B(k+1))+q_A(k+1)\cdot q_B(k+1)]}\cdot f \\ A_1(k+1)=\dfrac{\Delta i_B(k+1)\cdot f+A_0\cdot q_B(k+1)}{q_B(k+1)-1} \end{cases}$
(-1,1)	$\begin{cases} A_0(k+1)=\dfrac{\left[\Delta i_A(k+1)\cdot q_B(k+1)+\Delta i_B(k+1)\cdot(1-q_A(k+1))\right]\cdot f}{-[(1-q_A(k+1))\cdot(1-q_B(k+1))+q_A(k+1)\cdot q_B(k+1)]} \\ A_1(k+1)=\dfrac{\Delta i_B(k+1)\cdot f+A_0\cdot(1-q_B(k+1))}{q_B(k+1)} \end{cases}$
(-1,-1)	$\begin{cases} A_0(k+1)=\dfrac{\left[\Delta i_A(k+1)\cdot(1-q_B(k+1))-\Delta i_B(k+1)\cdot(1-q_A(k+1))\right]\cdot f}{q_B(k+1)-q_A(k+1)} \\ A_1(k+1)=\dfrac{\Delta i_B(k+1)\cdot f+A_0\cdot q_B(k+1)}{\left(q_B(k+1)-1\right)} \end{cases}$
$E_C(k+1)=1$	$q_C(k+1)=\dfrac{I_{ref}(k+1)\cdot f-i_C+A_0(k+1)}{A_1(k+1)+A_0(k+1)}$
$E_C(k+1)=-1$	$q_C(k+1)=\dfrac{(I_{ref}(k+1)-i_C)\cdot f+A_1(k+1)}{A_1(k+1)-A_0(k+1)}$

IV. SIMULATION VERIFICATION

To verify that the proposed control method can improve the comfort and safety of the high-power digital SRM drive system in EVs/HEVs applications, the proposed TSF based torque ripple reduction algorithm for an SRM drive system is implemented in MATLAB/SIMULINK.

The simulation parameters of the SRM are the same as the SRM parameters of the experimental platform, as shown in table II. A three-phase asymmetric half bridge power converter as shown in Fig. 2 is used.

TABLE II

SRM AND DRAG MOTOR PARAMETERS

Parameters	Value for the 12/8 SRM	Value for the tow permanent magnet motor
Phase number	3	3
Rated power P_e/kW	35	50
Maximum power P_e/kW	60	100
Rated voltage U_e/V	336	336
Rated current I_e/A	115	140
Rated speed n_e(rpm)	2000	1500
Stator/rotor poles	12/8	/
Type of cooling	Air	Water

In the simulations, the total torque reference is set as 60Nm. The SRM drive system works at two switching frequencies for active thermal management, 9.6 kHz and 4.8 kHz. The upper threshold frequency is selected according to the optimal efficiency and power of the switched reluctance motor. The lower threshold frequency is the lowest switching frequency that the proposed current controller can produce a similar current control performance as the traditional control method. One of these two switching frequencies is adopted depending on the power converter temperature. In the simulation results, i_a and U_A are phase current and phase voltage of phase A. T and T_{avg} are total instantaneous output torque and total average output torque. The torque ripple is defined as

$$T_{rip}=\frac{T_m-T_{avg}}{T_{avg}} \tag{15}$$

where T_m is the peak torque.

Fig. 9 shows the simulation waveforms of phase current,

phase voltage, total instantaneous output torque and total average output torque at 500rpm with switching frequency of 9.6 kHz.

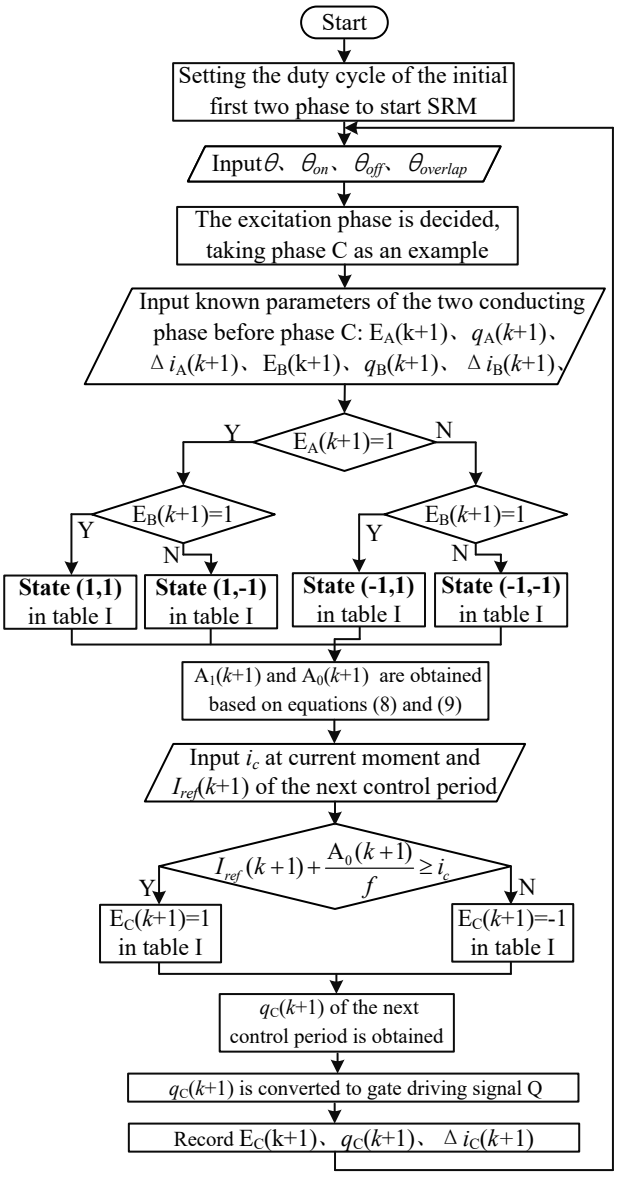

Fig.8 The flow chart of the digital implementation of the deadbeat control method

Fig. 9(a) is the simulation results without the proposed deadbeat current control, and the torque ripple is 25.2%. Fig. 9(b) is the simulation results with the proposed deadbeat current control method for TSF, and the torque ripple is reduced to 12% because of accurate current tracking.

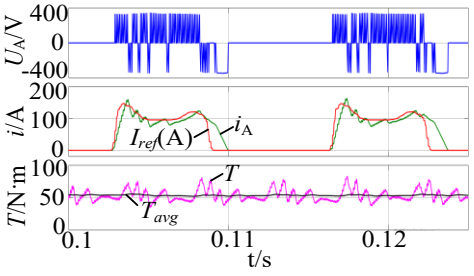

(a) TSF control without deadbeat current control

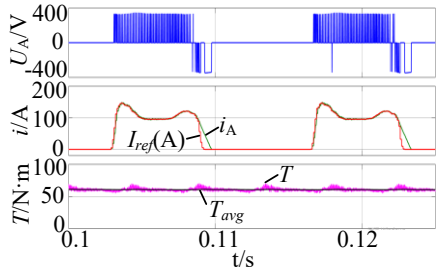

(b) The deadbeat control method for TSF

Fig.9 Simulation results for low-speed and normal switching frequency operation (n=500 rpm, *f*=9.6 kHz)

Fig. 10 shows the simulation results at a higher motor speed of 2000rpm. Similar conclusion as Fig. 9 can be obtained.

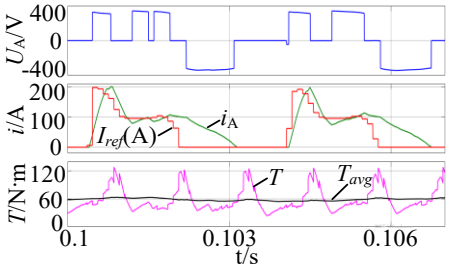

(a) TSF control without deadbeat current control

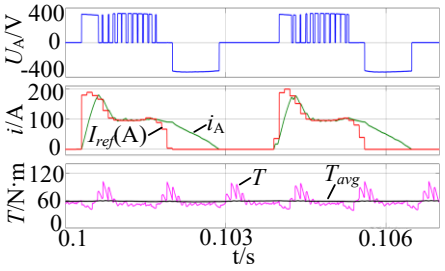

(b) The deadbeat control method for TSF

Fig.10 Simulation results for rated speed and normal switching frequency operation (n=2000 rpm, *f*=9.6 kHz)

Fig. 11(a) and Fig. 11(b) show the simulation results of switching frequency of 4.8 kHz at 500 rpm and 2000 rpm, respectively.

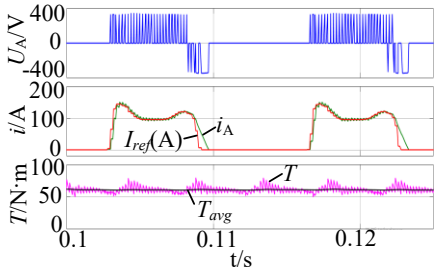

(a) Simulation results for low-speed (n=500 rpm)

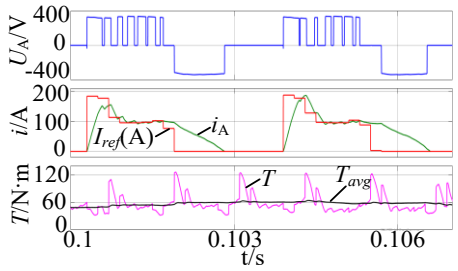

(b) Simulation results for rated speed (n=2000 rpm)

Fig.11 Simulation results for low switching frequency operation (f=4.8 kHz)

As shown in Fig. 11(a), the torque ripple is 25%. As shown in Fig. 11(b), the torque ripple is 77.5%. It can be concluded that the proposed deadbeat current control based TSF method can reduce SRM torque ripple, even if at low switching frequency. Therefore, the switching frequency can be reduced for active thermal management with little negative impact for the current and torque control performance.

As shown in Fig. 12(a), assuming the IGBT module is over temperature at t_1, and the switching frequency is reduced to 4.8 kHz from 9.6 kHz at 500rpm. As shown in Fig. 12(b), assuming the temperature of the IGBT module returns to normal at t_2, and the switching frequency rises to 9.6 kHz from 4.8 kHz.

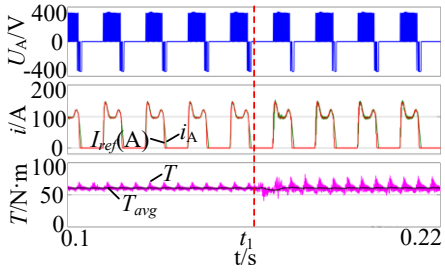

(a) Simulation results for frequency reduction

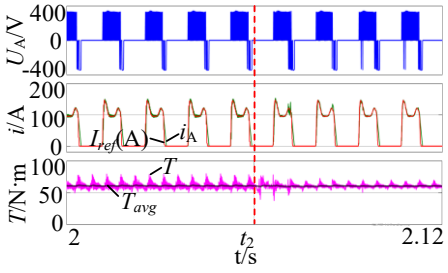

(b) Simulation results for frequency reduction

Fig.12 Simulation results for transition period of switching frequencies

From Fig. 12(a) and Fig. 12(b), it can be found that the torque and current can be controlled smoothly during the transition period of switching frequencies.

V. Experimental Result

In order to validate the feasibility and effectiveness of the proposed control method experimentally, an experimental system has been setup with the SRM parameters as shown in table II.

The experimental system is shown in Fig. 13. The proposed control methods are implemented in a Texas Instruments (TI)'s TMS320F28335DSP control board, and the current and voltage are observed using current clamp 700924 and voltage clamp 701930 of YOKOGAWA, respectively. The torque of SRM output is measured by torque meter JN338 from Beijing three crystal Joint Technology company with sampling frequency of 5 kHz-15 kHz. The real-time torque of SRM output can be sampled online. The instantaneous torque waveforms of SRM are shown by the recorder DL850 from YOKOGAWA combined with the frequency acquisition module 701281. The tow motor is operated in constant speed mode during the experiment.

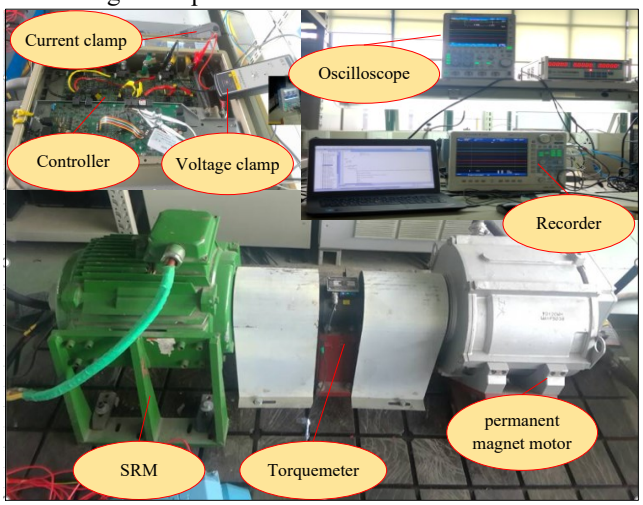

Fig.13 Experimental setup

In the experiment, the parameters such as turn-on angle, turn-off angle, overlapping angle were optimized, and the results of torque tracking at different speeds were obtained. The threshold frequencies are consistent with simulation model. At speed of 500 rpm, the experimental waveforms are shown in Fig. 14 with switching frequency being set to 9.6 kHz.

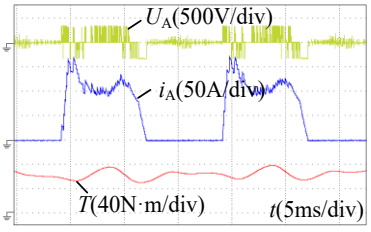

(a) TSF control without deadbeat current control

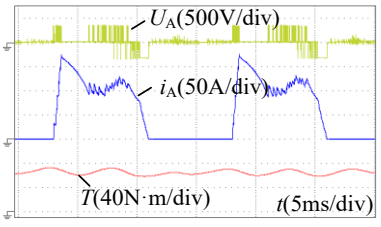

(b) The deadbeat control method for TSF

Fig.14 Experimental results for low-speed and normal switching frequency operation (n=500 rpm, f=9.6 kHz)

In Fig. 14(a), the traditional TSF control method is applied,

and the torque ripple is 25.2%. In Fig. 14(b), the deadbeat control method for TSF is applied, and the torque ripple is 12%. It shows that the proposed method can reduce the torque ripple of SRM significantly and improve the comfort of EVs/HEVs at low speed.

In the same way, in order to prove that the proposed method can obviously reduce the torque ripple of SRM at rated speed, experimental results are shown in Fig. 15 at 2000 rpm with switching frequency being set to 9.6 kHz.

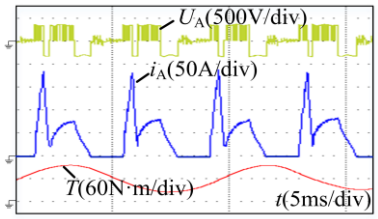

(a) TSF control without deadbeat current control

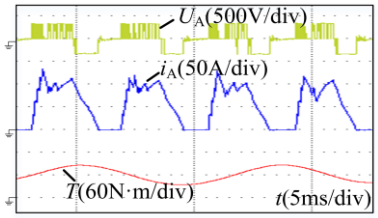

(b) The deadbeat control method for TSF

Fig.15 Experimental results for rated-speed and normal switching frequency operation (n=2000 rpm, f=9.6 kHz)

Fig. 15(a), the traditional TSF control method is applied, and the torque ripple is 57.5%. In Fig. 15(b), the deadbeat control method for TSF is applied, and the torque ripple is reduced to 42.5%. Thus, it validated that the proposed method can reduce the torque ripple of SRM and improve the comfort of EVs/HEVs at rated speed.

Fig. 16(a) and Fig. 16(b) show the experimental results of the proposed current controller with the switching frequency reduced to 4.8kHz at 500 rpm and 2000 rpm, respectively.

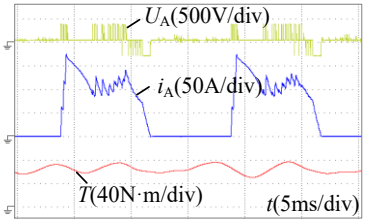

(a) Experimental results for low-speed (n=500 rpm)

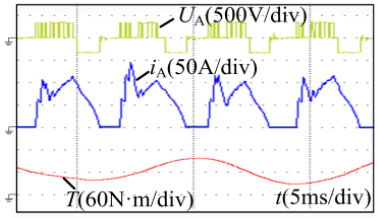

(b) Experimental results for rated-speed (n=2000 rpm)

Fig.16 Experimental results for low switching frequency operation (f=4.8 kHz)

As shown in Fig.16(a), the torque ripple is 22.2%. As shown in Fig.16(b), the torque ripple is 57%. It shows that the proposed method can still reduce torque ripple compared with traditional TSF, even if the switching frequency is reduced to half of the normal operation.

The comparison of simulation and experiment results is shown in table III. The torque waveforms shown in the experimental results have slight difference to the simulation results. It is because of the sampling frequency limitation of torque sensors, and the high frequency components of the torque ripples can't be measured in experiments.

TABLE III

COMPARISON OF SIMULATION AND EXPERIMENT RESULTS

	n(rpm)	f(kHz)	Control method	Ripple(%)
Simulation results	500	9.6	Without DBC	25.2
			DBC	12
		4.8	DBC	25
	2000	9.6	Without DBC	87
			DBC	52.5
		4.8	DBC	77.5
Experiment results	500	9.6	Without DBC	25.2
			DBC	12
		4.8	DBC	22.2
	2000	9.6	Without DBC	57.5
			DBC	42.5
		4.8	DBC	57

Fig. 17 shows the experimental results of torque ripple at rated and low speeds. From the figure, it can be found that proposed method can reduce the torque ripple of SRM significantly at rated and low speeds, even if at low switching frequency. Therefore, the switching frequency can be reduced with the proposed deadbeat current control without sacrificing the SRM control performance, which lead to that the lifetime of IGBT module can be prolonged, and switching loss can be reduced.

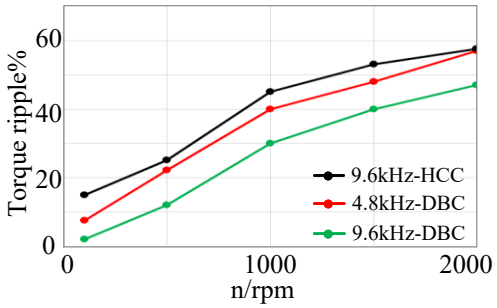

Fig.17 Experimental results of torque ripple at rated and low speeds

As shown in Fig. 18(a), in order to reduce the temperature of the power converter at t'_1, the switching frequency is reduced to 4.8 kHz from 9.6 kHz at 500rpm. As shown in Fig. 18(b), when the temperature of the IGBT module is relatively

low, the output performance of SRM can be improved by rising the switching frequency to 9.6kHz from 4.8kHz.

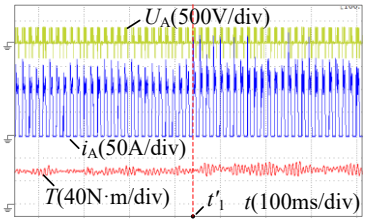

(a) Experimental results for frequency reduction

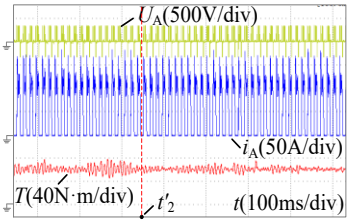

(b) Experimental results for frequency recovery

Fig.18 Experimental results for transition period of switching frequencies

From Fig. 18(a) and Fig. 18(b), it can be found that the torque ripple will not mutate at the moment of the switching frequency conversion, and the SRM can achieve smooth frequency transition.

At speed of 500 rpm, the experimental waveforms of active thermal management are shown in Fig. 19. In Fig. 19(a), the total torque reference is set as 60Nm, and the switching frequency is reduced to 4.8 kHz from 9.6 kHz at t'_3. In Fig. 19(b), the total torque reference is set as 80Nm, and the switching frequency is reduced to 4.8 kHz from 9.6 kHz at t'_4.

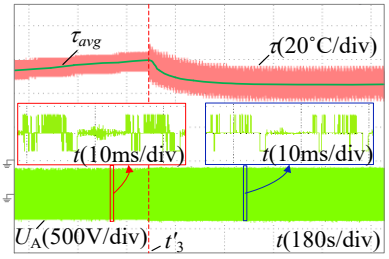

(a) Experimental results with torque reference being set as 60Nm

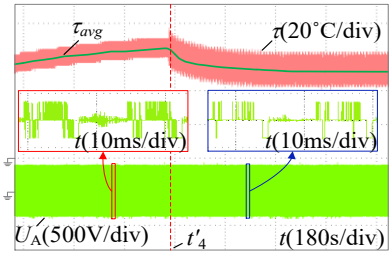

(b) Experimental results with torque reference being set as 80Nm

Fig.19 Experimental results for active thermal management

The specific temperature values of the experimental results are shown in table IV. These specific temperature values include the average temperature τ_{javg}, the maximum temperature τ_{jmax} and the minimum temperature τ_{jmin} under steady state of temperature corresponding to different switching frequency. Additionally, the time required for the transition of temperature from one steady state to another is also included.

TABLE IV

EXPERIMNTAL RESULTS FOR ACTIVE THERMAL MANAGEMENT

	Time of the transition (s)	f(kHz)	τ_{javg}(°C)	τ_{jmax}(°C)	τ_{jmin}(°C)
60Nm	565	9.6	59	64.5	52.8
		4.8	45.2	53.4	36.9
80Nm	591	9.6	65	70.7	58.6
		4.8	51.7	61	43

From Fig. 19 and table IV, it can be found the steady state temperature of the power converter at 80Nm torque reference with the switching frequency of 4.8 kHz is lower than that at 60Nm with 9.6 kHz switching frequency. Therefore, the power converter can be protected from over-temperature failure by reducing the switching frequency, when the output torque of the SRM needs to be increased under some operating conditions, such as sudden increase of the EVs/HEVs load and climbing section.

VI. CONCLUSION

This paper presented a switched reluctance motor control strategy with torque ripple reduction and active thermal management. The working principle and digital realization of the proposed method have been introduced in detail. Additionally, the simulation results and experimental results are presented. It can be concluded that the proposed method can protect IGBT module from over-temperature failure by reducing the switching frequency and thus the safety of EVs/HEVs can be improved. Additionally, the proposed deadbeat current control method can improve the SRM current control accuracy, so that SRM torque control error can be reduced significantly.

REFERENCES

[1] Yihua Hu, Chun Gan, Wenping Cao, Wuhua Li, and Stephen J. Finney, "Central-Tapped Node Linked Modular Fault-Tolerance Topology for SRM Applications," IEEE Trans. Power Electron., vol. 31, no. 2, pp. 1541-1554, Feb. 2016.

[2] B. Ji, X. Song, W. Cao, V. Pickert, Y. Hu, J. W. Mackersie, and G. Pierce, "In situ diagnostics and prognostics of solder fatigue in IGBT modules for electric vehicle drives," IEEE Trans. Ind. Appl., vol. 48, no. 6, pp. 2287-2295, Nov./Dec. 2012.

[3] S. P. Nikam, V. Rallabandi, and B. G. Fernandes, "A High-Torque-Density Permanent-Magnet Free Motor for in-Wheel Electric Vehicle Application," IEEE Trans. Power Electron., vol. 28, no. 12, pp. 5489-5498, Dec. 2013.

[4] A. Chiba, K. Kiyota, N. Hoshi, M. Takemoto, S.

Ogasawara, “Development of a rare-earth-free SR motor with high torque density for hybrid vehicles,” IEEE Trans. Energy Convers., vol. 30, no. 1, pp.175-182, Mar. 2015.
[5] X. D. Xue *et al.*, “Optimal control method of motoring operation for SRM drives in electric vehicles,” IEEE Trans. Veh. Technol., vol. 59, no. 3, pp. 1191–1204, Mar. 2010.
[6] A. Chiba, M. Takeno, N. Hoshi, M. Takemoto, S. Ogasawara, and M. A. Rahman, “Consideration of number of series turns in switched reluctance traction motor competitive to HEV IPMSM,” IEEE Trans. Ind. Appl., vol. 48, no. 6, pp. 2333–2340, Nov./Dec. 2012.
[7] R. Madhavan and B. G. Fernandes, “Axial flux segmented SRM with a higher number of rotor segments for electric vehicles,” IEEE Trans. Energy Convers., vol. 28, no. 1, pp. 203–213, Mar. 2013.
[8] E. Annie Elisabeth Jebaseeli and S. Paramasivam, “Prediction of thermal behaviour of Switched Reluctance Machine using Regression Technique,” in Proc. IEEE ICECCT, Mar. 5–Mar. 7, 2015, pp. 1–5.
[9] A. H. Isfahani and B. Fahimi, “Comparison of mechanical vibration between a double-stator switched reluctance machine and a conventional switched reluctance machine,” IEEE Trans. Magn., vol. 50, no. 2, Feb. 2014, Art. ID 7007104.
[10] D. H. Lee, T. H. Pham, and J.-W. Ahn, “Design and operation characteristics of four-two pole high-speed SRM for torque ripple reduction,” IEEE Trans. Ind. Electron., vol. 60, no. 9, pp. 3637–3643, Sep. 2013.
[11] R. C. Kavanagh, J. M. D. Murphy, and M. G. Egan, “Torque ripple minimization in switched reluctance drives using self-learning techniques,” in Proc. IEEE IECON, Oct. 28–Nov. 1, 1991, pp. 289–294.
[12] D. H. Lee, Z. G. Lee, and J. W. Ahn, “A simple nonlinear logical torque sharing function for low-torque ripple SR Drive,” IEEE Trans. Ind. Electron., vol. 56, no. 8, pp. 3021–3028, Aug. 2009.
[13] I. Husain, “Minimization of torque ripple in SRM drives,” IEEE Trans. Ind. Electron., vol. 49, no. 1, pp. 28–39, Feb. 2002.
[14] S. K. Sahoo, S. K. Panda, and J. Xu, “Indirect torque control of switched reluctance motors using iterative learning control,” IEEE Trans. Power Electron., vol. 20, no. 1, pp. 200–208, Jan. 2005.
[15] S. K. Sahoo, S. K. Panda, and J. Xu, “Iterative learning-based high performance current controller for switched reluctance motors,” IEEE Trans. Energy Convers., vol. 19, no. 3, pp. 491–498, Sep. 2004.
[16] N. Chayopitak, R. Pupadubsin, and K. Tungpimolrut, “An online lowripple torque control of switched reluctance motor for small electric vehicle,” in Proc. Int. Conf. Elect. Mach. Syst., Wuhan, China, 2008, pp. 3327–3332.
[17] S. Y. Ahn, J. W. Ahn, and D. H. Lee, “A Novel torque controller design for high speed SRM using negative torque compensator,” in Proc. Int. Conf. Power Electron. Energy Convers. Congr. Expo., Jeju, Korea, 2011, pp. 937–944.
[18] M. Dowlatshahi, S. M. S. Nejad, and J. W. Ahn, “Torque ripple minimization of switched reluctance motor using modified torque sharing function,” in Proc. IEEE Iranian Conf. Elect. Eng., Mashhad, Iran, 2013, pp. 1–6.
[19] Jin Ye, Berker Bilgin, and Ali Emadi, “An offline torque sharing function for torque ripple reduction in switched reluctance motor drives,” IEEE Trans. Energy Convers., vol.30, no.2, pp.726-735, Jan. 2015
[20] Hao Wen, and Zaiping Pan, “A Novel Dead-Beat Torque Control of Switched Reluctance Machines,” in Proc. IEEE International Conference on Electrical Machines and Systems, Aug. 20-Aug. 23, 2011, pp. 1-5.
[21] Athar Hanif, Aamer I. Bhatti, and Qadeer Ahmed, “Managing Thermally Derated Torque of an Electrified Powertrain Through LPV Control,” IEEE Trans. Mechatronics, vol. 23, no. 1, pp. 364–376, Feb. 2018.
[22] Jin Ye, Pawel Malysz, and Ali Emadi, “A Fixed-Switching-Frequency Integral Sliding Mode Current Controller for Switched Reluctance Motor Drives,” IEEE Journal of Emerging and Selected in Power Electronics, vol. 3, no. 2, pp.381-394, Sep. 2014.
[23] Zhiyu Sun, Mingyao Ma, Mingyue Zhan, and Jianing Wang, “Junction temperature estimation in IGBT power modules based on Kalman filter,” in Proc. IEEE EI2, Nov. 26–Nov. 28, 2017, pp. 1–6.
[24] “FF600R12ME4 Datasheet,” https://pdf1.alldatasheet.com/datasheet-pdf/view/417216/INFINEON/FF600R12ME4.html

Xing Zhang (M’13–SM’14) received the B.S., M.S., and Ph.D. degrees in electrical engineering and automation from Hefei University of Technology, Hefei, China, in 1984, 1990, and 2003, respectively. Since 1984, he has been a Faculty Member with the School of Electric Engineering and Automation, Hefei University of Technology, where he is currently a Professor. He is also with the Photovoltaic Engineering Research Center of the Ministry of Education. His main research interests include photovoltaic generation technologies, wind power generation technologies, and distributed generation systems.

Qingqing Yang (S’16) received the B.S. degree in electrical engineering from the Hefei University of Technology, Hefei, China, in 2014. She is currently pursuing the Ph.D. degree in electrical engineering with the Hefei University of Technology, Hefei, China. Her main research projects are torque ripple suppression and advanced algorithms of switched reluctance motor.

Mingyao Ma (M'11) received the B.Sc. and Ph.D. degrees in applied power electronics and electrical engineering from Zhejiang University, Hangzhou, China, in 2004 and 2010, respectively. From October 2008 to October 2009, she was a visiting PhD postgraduate research student in the University of Strathclyde, Glasgow, U.K., and in 2010, she joined Zhejiang University as a Post-Doctoral Research Fellow. In 2011, she worked for the University of Central Florida, Orlando, US, as the visiting scholar. From April 2012 to April 2015, she joined the Newcastle University, Newcastle, UK, as the Research Associate. From 2015 she works in Hefei University of Technology as a professor. Her research interests include fault diagnostic technology for PV generation system, SR motor control, and health monitoring of power electronics systems.

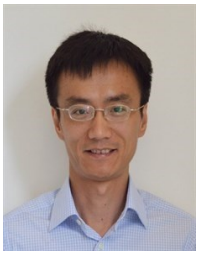

Zhengyu Lin (M'05–SM'10) received the B.Sc. and M.Sc. degrees from the College of Electrical Engineering, Zhejiang University, Hangzhou, China, in 1998 and 2001, respectively, and the Ph.D. degree from Heriot-Watt University, Edinburgh, U.K. in 2005.

He is currently a Senior Lecturer in School of Mechanical, Electrical and Manufacturing Engineering with Loughborough University, Loughborough, U.K. He was an R&D Engineer with Nidec Control Techniques from 2006 to 2011, a Senior Research Scientist with Sharp Laboratories of Europe Ltd. from 2011 to 2012, and a Lecturer with Aston University from 2014 to 2019. His research interests include power electronics and its applications in renewable energy, energy storage, motor drives and microgrids.

Shuying Yang (M'13) received the B.S. and Ph.D. degrees in automation and electrical engineering from the Hefei University of Technology (HFUT), Hefei, China, in 2002 and 2008, respectively. He joined the teaching faculty of the School of Electrical Engineering and Automation, HFUT, in 2005. From August 2014 to October 2015, he served as a Visiting Scholar with the University of New Brunswick, Fredericton, NB, Canada. He is currently a Professor with HFUT. His research interests and experience include renewable energy conversion, electrical drives, and application of control theory.